



# Ultrathin graphitic $C_3N_4$ nanosheets as highly efficient metal-free cocatalyst for water oxidation



Chenchen Feng, Zhonghao Wang, Ying Ma, Yajun Zhang, Lei Wang, Yingpu Bi\*

State Key Laboratory for Oxo Synthesis & Selective Oxidation, National Engineering Research Center for Fine Petrochemical Intermediates, Lanzhou Institute of Chemical Physics, CAS, Lanzhou, Gansu 730000, China

## ARTICLE INFO

### Article history:

Received 8 September 2016

Received in revised form

26 November 2016

Accepted 6 December 2016

Available online 7 December 2016

### Keywords:

$BiVO_4$

Co-catalyst

Water oxidation

## ABSTRACT

Here, we demonstrate that ultrathin graphitic-phase  $C_3N_4$  nanosheets (g- $C_3N_4$ -NS) could serve as an efficient metal-free cocatalyst for improving oxygen evolution activity on nanoporous  $BiVO_4$  photoanode. More specifically, as compared with pure  $BiVO_4$  photoanode, ultrathin g- $C_3N_4$  nanolayers not only suppress the surface charge recombination of  $BiVO_4$ , but also effectively transfer and store holes for water oxidation. As expected, the ultrathin graphitic-phase  $C_3N_4$  cocatalyst modified  $BiVO_4$  photoanode exhibited significantly improved photocurrent density and  $H_2$  generation capability, nearly 7 and 12 times with respect to the pristine  $BiVO_4$  under the same conditions. These results demonstrate an effective approach for the design and construction of low-cost and highly efficient PEC systems.

© 2016 Elsevier B.V. All rights reserved.

## 1. Introduction

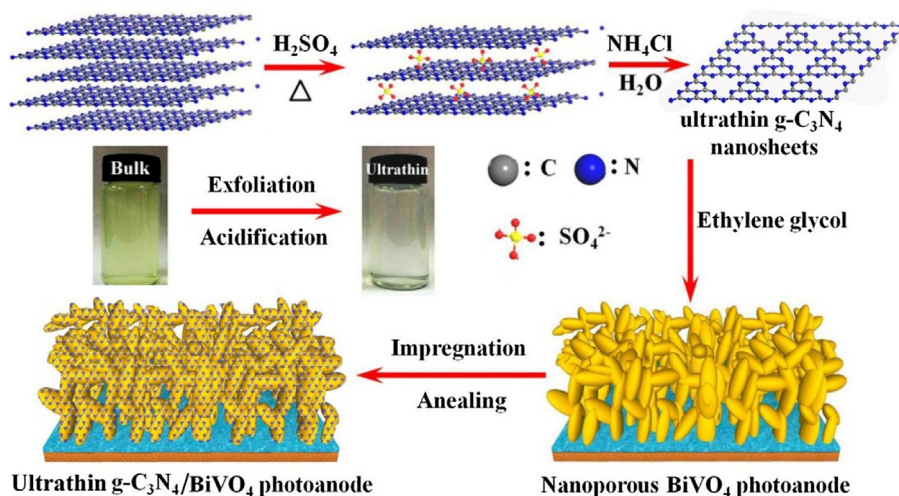
Photoelectrochemical (PEC) water splitting is a potentially scalable approach to store solar energy in the form of clear and renewable  $H_2$  fuel [1–4]. Among various semiconductors, *n*-type monoclinic bismuth vanadate ( $BiVO_4$ ), with a moderate band gap matching well with solar spectrum, has recently emerged as a promising photoanode material for PEC water-splitting [5–13]. However, the PEC performance for water oxidation is far below that expected owing to the intrinsically sluggish kinetics of the oxygen evolution reaction (OER) dominated by photogenerated holes. In this regards, various strategies, including metal ions doping [14–17], hetero-coupling [18–21], and cocatalyst deposition [8–11,22,23], have been extensively employed to improve the performances of  $BiVO_4$ -based photoanodes. Particularly, depositing *p*-type VIII metal (Fe, Co, Ni) oxide or (oxy) hydroxide with reversible redox properties, which have been extensively utilized as electrocatalysts for water oxidation, has been proved to be a more effective approach to accelerate the surface charge separation as well as minimize the kinetic over potential [11,24,25]. More specifically, the photogenerated holes could be extracted from the  $BiVO_4$  bulk and stored in the *p*-type cocatalysts for suppressing electron-hole recombination. Recently, Gong et al. [22] demonstrated that the loading *p*- $Co_3O_4$  particles on  $BiVO_4$  photoanodes

enables simultaneous enhancement of surface reaction kinetics and bulk charge separation. Gamelin et al. [15] modified *W*:  $BiVO_4$  photoanode surfaces with Co-Pi catalyst, which yielded a large cathodic shift ( $\sim 440$  mV) in the onset potential for PEC water oxidation. Choi et al. [9–11] reported that the loading *p*-type FeOOH and NiOOH dual-layers onto  $BiVO_4$  photoanodes could greatly improve the PEC performances. Domen et al. [23] reported that dual cocatalysts of  $CoO_x$  and NiO loaded  $BiVO_4$  photoanodes enables a 1.5% half-cell solar-to-hydrogen efficiency for the water oxidation. Although these *p*-type VIII metal cocatalysts could effectively enhance the PEC properties of  $BiVO_4$  photoanodes, but the metallic ions containing materials with perceptive toxicity definitely hampered their further applications. Moreover, their usual large thicknesses or dimensions may block sunlight absorption and prolong the holes transport distances. Thereby, the exploration of novel *p*-type metal-free co-catalysts with ultrathin structures may be an alternative strategy for enhancing the PEC performances of  $BiVO_4$  photoanodes.

As a typical *p*-type metal-free semiconductor, graphitic-phase carbon nitride (g- $C_3N_4$ ) with a graphite-like layered structure has been extensively applied in photocatalytic hydrogen generation [26–29], degradation of organic pollutants [30–33], electrochemical sensors [34,35], and biomedical imaging [36], owing to its appropriate bandgap (2.7 eV), thermal and chemical stability, and nontoxic properties. However, the applications for water oxidation over g- $C_3N_4$  have been rarely reported as a result of its relatively low position of valence bands. Furthermore, the direct charge transfer across g- $C_3N_4$  layer is difficult as a result of the graphite-

\* Corresponding author.

E-mail address: [yingpubi@licp.cas.cn](mailto:yingpubi@licp.cas.cn) (Y. Bi).



**Scheme 1.** Schematic illustration of the exfoliation and acidification process for fabricating ultrathin  $g\text{-C}_3\text{N}_4$  nanosheets and  $\text{BiVO}_4/g\text{-C}_3\text{N}_4\text{-NS}$  photoanodes.

like layered structure with weak van der Waals force. More recently, both theoretical and experimental studies demonstrated that  $g\text{-C}_3\text{N}_4$  possesses a unique thickness-dependent bandgap, and ultrathin thick 2D nanosheets can effectively enlarge the bandgap with respect to bulk materials, which is attributed to the well-known quantum confinement effect by shifting the conduction and valence band edges in opposite directions [33,34,37–39]. Moreover, owing to the ultrathin layered structure, the  $g\text{-C}_3\text{N}_4$  nanosheets demonstrated impressive carrier mobility and were extensively applied in various electronic and optoelectronic devices [40]. Thereby, reducing the bulk 3D  $g\text{-C}_3\text{N}_4$  into ultrathin 2D nanosheets and coating on photoanodes as co-catalysts may not only facilitate the rapid hole transfer from their contact interfaces, but also enhance the oxygen oxidation capability due to the enlarged valence band.

Herein, we demonstrate a simple ethylene glycol dispersion and impregnation method for uniform coating ultrathin  $g\text{-C}_3\text{N}_4$  nanosheets ( $g\text{-C}_3\text{N}_4\text{-NS}$ ) on nanoporous  $\text{BiVO}_4$  photoanodes. More specifically, ultrathin  $g\text{-C}_3\text{N}_4\text{-NS}$  could effectively suppress the surface charge recombination on the  $\text{BiVO}_4$ , and photogenerated holes could be effectively stored on their valence band for water oxidation. Nyquist curves further demonstrated that the ultrathin  $g\text{-C}_3\text{N}_4$  structure could greatly increase the charge-carrier density and facilitate more efficient electron-hole separation. As expected, the ultrathin  $g\text{-C}_3\text{N}_4\text{-NS}$  loading  $\text{BiVO}_4$  photoelectrodes exhibit superior photoelectrochemical water oxidation in terms of onset potential, photocurrent density and  $\text{H}_2$  generation capability as compared with pure as well as metal electrocatalysts modified  $\text{BiVO}_4$  electrodes.

## 2. Results and discussion

**Scheme 1** shows the synthesis process of ultrathin  $g\text{-C}_3\text{N}_4\text{-NS}$  as well as their coating on nanoporous  $\text{BiVO}_4$  photoanodes in this work. Briefly, ultrathin  $g\text{-C}_3\text{N}_4\text{-NS}$  was prepared by an acidification oxidation and exfoliation process for bulk  $g\text{-C}_3\text{N}_4$ , and finally dispersed in ethylene glycol solvent [41,42], which is crucial for the subsequent loading on nanoporous  $\text{BiVO}_4$  photoanodes. The X-ray diffraction pattern of  $g\text{-C}_3\text{N}_4\text{-NS}$  (Fig. S1B) is consistent with the bulk  $g\text{-C}_3\text{N}_4$ , suggesting that the nanosheets basically possess the same crystal structure as the bulk  $g\text{-C}_3\text{N}_4$ . With respect to the bulk  $g\text{-C}_3\text{N}_4$ , the peak originated from the periodic stacking of layers in the nanosheets is shifted from  $27.34^\circ$  to  $27.98^\circ$ , indicating a decreased gallery distance between the nanosheets [27,28]. The

UV–vis absorption spectrum of  $g\text{-C}_3\text{N}_4\text{-NS}$  (Fig. S2A) clearly shows an obvious blue shift of the intrinsic absorption edge with respect to the bulk  $g\text{-C}_3\text{N}_4$ . The derived bandgap from the plot versus the energy of the absorbed light (Fig. S2B) is 3.03 eV for the ultrathin nanosheets, which is larger than the bulk material of 2.75 eV. The band structure of  $g\text{-C}_3\text{N}_4$  and pure  $\text{BiVO}_4$  has been tested and calculated. Besides, the band structure of the heterostructure has been shown in Fig. S3.

**Fig. 1A** shows the typical transmission electron microscope (TEM) image of the  $\text{BiVO}_4/g\text{-C}_3\text{N}_4\text{-NS}$  sample. The nanoporous  $\text{BiVO}_4$  photoanodes have been coated by ultrathin  $g\text{-C}_3\text{N}_4$  nanolayers, and no evident bulk structure as a result of self-agglomeration have been observed. The high resolution TEM image in **Fig. 1B** exhibits that ultrathin  $g\text{-C}_3\text{N}_4$  nanolayers with a thickness of 2 nm have been compactly attached on the surfaces of monoclinic  $\text{BiVO}_4$  nanocrystals. Moreover, both carbon and nitrogen elements were detected in the whole regions from the elemental mapping images (**Fig. 1C**) and elemental line scanning (**Fig. S4**), which confirm the uniform dispersion of a  $g\text{-C}_3\text{N}_4$  nanolayers on the surfaces of nanoporous  $\text{BiVO}_4$ . However, as compared with pure nanoporous  $\text{BiVO}_4$  sample as shown in **Fig. S5**, the SEM images (**Fig. 1D** and **E**) and XRD patterns (**Fig. 1F**) demonstrated no evident crystals structure or morphology change, which should be due to the uniform dispersion and ultrathin thickness of  $g\text{-C}_3\text{N}_4$  nanosheets. Besides, the fourier transform infrared (FT-IR) spectra have also been performed. As shown in **Fig. S6**, the basic peaks of  $g\text{-C}_3\text{N}_4$  have been clearly observed in the as-prepared samples [29,33]. The UV–vis diffuse reflectance spectra (DRS) were utilized to investigate the band gap energy ( $E_g$ ) values of the crystals (**Fig. S2**). As a result of large direct bandgap energy (3.03 eV) of ultrathin  $g\text{-C}_3\text{N}_4\text{-NS}$ , the absorption edge and intensity of  $\text{BiVO}_4/g\text{-C}_3\text{N}_4\text{-NS}$  are generally consistent with pure  $\text{BiVO}_4$  with direct band gap energy ( $E_g$ ) of 2.48 eV. On the basis of above results, it can be confirmed that ultrathin  $g\text{-C}_3\text{N}_4$  nanosheets could be successfully and uniformly coated on the  $\text{BiVO}_4$  photoanodes by this simple impregnation process.

**Fig. 2** shows the high-resolution C1 s and N1 s spectra of  $g\text{-C}_3\text{N}_4\text{-NS}$  and  $\text{BiVO}_4/g\text{-C}_3\text{N}_4\text{-NS}$ . The C1 s spectra (**Fig. 2A**) shows two deconvoluted peaks at 288.6 eV and 284.8 eV, ascribed to the signals of  $\text{sp}^2$ -bonded carbon ( $\text{N}=\text{C}=\text{N}$ ) and standard reference carbon, which is usually observed in the XPS spectrum of carbon nitrides. In **Fig. 2B**, the high resolution N1 s spectra can be also deconvoluted into three different peaks. The N1 s peak at 398.9 eV corresponds to  $\text{sp}^2$  hybridized aromatic N bonded to carbon atoms ( $\text{C}=\text{N}-\text{C}$ ). The peak at 399.7 eV is assigned to the tertiary N bonded to carbon

Download English Version:

<https://daneshyari.com/en/article/6454280>

Download Persian Version:

<https://daneshyari.com/article/6454280>

[Daneshyari.com](https://daneshyari.com)